Chapter 4

Alternative Confinement Vessels for Fusion Power

4.1 Stellarator Machines Eliminate the Mega–Amperes of Plasma Currents by Using Nonsymmetric Magnetic Field Configurations

Max-Planck Institute for Plasma Physics first in Garching and now in Greifswald, Germany

4.2 The Greifswald Stellarator machine W7X makes a breakthrough with 10 KeV hydrogen plasma driven by high–power RF heating avoiding the Mega–Amperes of plasma currents

Wendelstein 7–X (W7–X) was operated successfully with the first divertor plasma in the operation phase 1.2a (OP1.2a). A new combined probe head, developed and installed on the multiple–purpose manipulator, is able to measure the edge plasma profiles ($T_e, n_e, \phi_f, M_\parallel$), variation of magnetic field, poloidal and radial turbulence structures. The Scrape–Off Layer (SOL) plasma parameters in two magnetic configurations (standard and high mirror) are in good agreement with the magnetic island structure and the field line connection length calculated by the field line tracer. In both the standard and high mirror configurations, the radial turbulent heat flux and particle flux have strong dependence on the local magnetic topology, revealing two distinct transport patterns: a broadband turbulence dominant region in the outer SOL and a low–frequency dominant region in the inner SOL. In the standard divertor configuration, the broadband turbulence with

a frequency range of 40-120 kHz is located near the island center along the probe path, leading to outward transport. These broadband fluctuations propagate with a velocity of 2.3-4.6 km/s poloidally along the ion diamagnetic drift direction in the plasma frame, with $k_\theta \rho_s$, close to 0.1. The large radial transport induced by the broadband turbulence is accompanied by a steep electron density gradient. The low frequency (0-30 kHz) dominant transport exhibits obvious intermittent structure. Some statistical techniques are applied to the characterization of the intermittent transport.

4.3 Large Helical Device (LHD) Produces Fusion Power in Japan

4.3.1 Helical Magnetic Confinement System Invented in Japan — the Large Helical Device (LHD) Produces Fusion Power Deuterium Plasma for 30–minute Steady States

Both the early intro–ELM and inter–ELM periods produce inputs of tungsten and beryllium ions into the core plasma under a variety of conditions. Theoretical modeling and comparisons with data from the fusion tokamaks WEST, EAST, KSTAR (Korea Superconducting Tokamak Advanced Research), JET (Joint European Torus) and DIII–D (Doublet III) show that the inward fluxes of impurity ions and their accumulation conditions are critical issues for ITER. *Michoski, et al.* (2017) and *Michoski and Horton* (2019) used theoretical models and simulations for the vessel–wall emission problem combined with drift wave impurity transport formulas. The models interpret the spectroscopic emission data produced by the impurity ions and dust particles crossing the magnetic separatrix to enter the core plasma in tokamaks and in the Large Helical Device. The research produces models for the rate of accumulations of Be and W ions during an ELM event and during minor disruptions. A set of impurity transport equations is solved using formulas for impurity fluxes driven by drift waves with ion particles and hydrogen isotopes. The spectral emission work extends the earlier models from the Alcator C–MOD impurity transport research [*Rowan, et al.* (2008)] and recent applications to DIII–D impurity injection transport experiments [*Houshmandyar, et al.* (2016, 2018), *Michoski, et al.* (2017), *Michoski and Horton* (2019)].

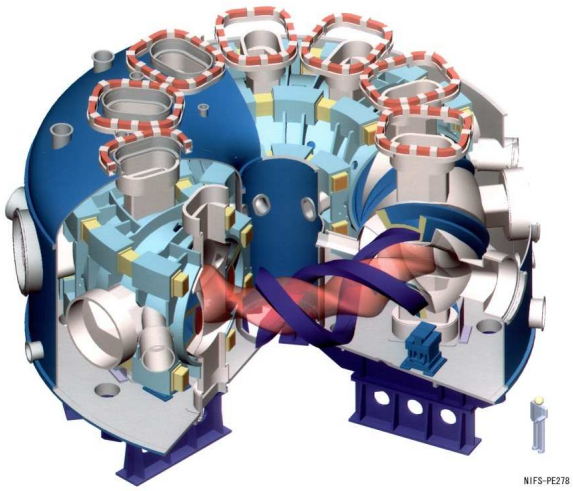

Figure 4.1: The Large Helical Device with the helical coils in black that surround the large helical plasma shown in gray. There are fourteen injection chambers around the top and around the outside of the torus to drive the hour–long steady–state plasmas.

Research extending the earlier development of models for inward turbulent transport of impurities from the first wall and the divertor walls [*Don, et al.* (1999), *Futatani, et al.* (2010)] is carried out with experiments in WEST with tungsten divertor walls. Large Helical Device (LHD) data with hydrogen plasmas shows the inward transport of plasma dust particles from 100 nm to microsized dust particles. The physics of these large negatively–charged dust grains is similar to that of dust transport in deserts of West Texas is closely related to the charged SiO_2 dust that rises from solar heating in Dust Devils. The dust devil models and the codes [*Onishchenko, et al.* (2014)] are generalized to the plasma dust transport problem.

The LHD plasmas provide a data set for comparison with simulations. Studies called TESPEL for dust transport in the WEST and EAST deuterium plasmas. The TESPEL data from *Nakamura, et al.* (2017) in the Large Helical Device (LHD) injects microsized plastic balls containing the elements with neighboring atomic numbers to the iron and chromium atoms in the vessel walls — namely the three tracer elements $V(Z = 23), Mn(Z = 25)$ and $Co(Z = 27)$ described in *Nakamura, et al.* (2014).

A major effort in the machine design has been that of producing a plasma column in which a high mean poloidal field $\overline{B}_p \simeq \sqrt{10}\,\mathrm{T}$ can be reached together with plasma currents $I_p \simeq$ 10-11 MA while maintaining reasonable safety factors against the onset of macroscopic instabilities (i.e. $q(\psi_a) \simeq 3.6$). The rough arguments for this choice of objectives are as follows: High values of the confinement parameter $n\tau_E, n$ being the particle density and τ_E the energy replacement time, should be reached considering that the maximum particle density should be related to the average current density $\langle J_\parallel \rangle \sim \overline{B}_p/\overline{a}$, where $\overline{a}$ is the mean plasma minor radius, and that the confinement time should have a significant dependence on I_p. Then the maximum values of $n\tau_E$ should be related to $\overline{B}_p^2$ as $I_p \simeq 5\overline{a}\overline{B}_p$. Moreover, if we consider the mean plasma pressure to be limited by the magnetic pressure $\overline{B}_p^2/(2\mu_0)$, the plasma reactivity represented by $n^2\langle\sigma_f v\rangle \propto n^2T^2$ can be

expected to be related to $\overline{B}_p^4$. These considerations have in fact been supported by sophisticated numerical simulations that have been carried out by 1+1/2D transport codes [*Coppi, et al.* (2010, 2013), *Airoldi and Cenacchi* (1997)]. In this connection we observe that well–confined plasmas with maximum densities close to $10^{21}\,\mathrm{m}^{-3}$ have been obtained repeatedly by the Alcator line of experiments and, with lower temperatures, by the Large Helical Device machine. To facilitate the attainment of these densities, the adoption, as in the case of the Alcator C experiments, of a pellet injector is planned. In the case of IGNITOR, however, the required pellet speeds are considerably higher and further advances (expected to be possible) in the technology of these injectors are needed.

4.3.2 Local turbulence measurements in the Large Helical Device by phase contrast imaging

Two–dimensional phase contrast imaging (2D) installed on the Large Helical Device (LHD) is a unique diagnostic for local turbulence measurements. Using a 10.6 micron infrared CO_2 laser and a 6×8 channel HgCdTe 2D detector are used. The length of the scattering volume is larger than plasma size. However, the asymmetry of turbulence structure with respect to the magnetic field and magnetic shear make local turbulence measurements possible. From a 2D image of the integrated fluctuations, the spatial cross–correlation function is estimated using time domain correlation analysis, then, the integrated 2D k–spectrum is obtained using maximum entropy method.

The 2D k–spectrum is converted from Cartesian coordinates to cylindrical coordinates. Finally, the angle in cylindrical coordinate is converted to flux surface labels. The fluctuation profile over almost the entire plasma diameter can be obtained at a single moment. The measurable k–region can be varied by adjusting the detection optics. In the LHD plasma, $k = 1 - 10\,\mathrm{cm}^{-1}$ fluctuations are measured which is expected region of ion temperature gradient and trapped electron turbulence in LHD. The spatial resolution is 10%–50% of the plasma minor radius [*Tanaka, et al.* (2008)].

4.3.3 Dense core plasmas in LHD and internal transport barriers

The Large Helical Device (LHD) [*Nakamura, et al.* (2014, 2017), *Yoshinuma, et al.* (2010)] has achieved high–density plasmas with Internal Transport Barriers (ITB) — also called Internal Diffusion Barriers — in the LHD research program at the National Institute of Fusion Science (NIFS). The core plasma density and pressure exceeded $10^{21}\mathrm{m}^{-3}$ and 150 kPa in 1989 with an internal transport barrier. The foot point of the Internal Diffusion Barrier extends to the last closed magnetic surface at $k_{\max \mathrm{n_e}} = 3.9$ to 4.0 m.

4.4 Linear Fusion Machines Designed by Norman Rostoker Produce Record Mirror–Confined Plasmas

4.5 Gamma 10 Mirror–Confined Plasmas

The electric potential experiments on GAMMA–10 [*Cho, et al.* (2008)] are consistent with the potential results on the Norman (TAE–x) field–reversed plasmas. The mirror plasma–parameter improvement is essential. The Internal Transport Barrier (ITB) and H–mode pedestal in tokamaks has similar physics enhancing the plasma confinement.

In the central cell of GAMMA–10 the ECH injection raises T_e from 100 eV to 1000 eV in association with an increase in the ion temperature T_i from 500 eV to 1 KeV because of a significant reduction of electron drag from KeV electron temperature and the ICH ion heating produced by hot ions in the central cell with $T_i \sim 1$ KeV. The ECH heating level was $P_{\rm ECH} \leq 170$ kW [*Pratt and Horton* (2006)].

The experiments showed that ECH heating with high–power gyrotrons for bulk electron heating may produce plasma with fusion–grade parameters.

Tandem mirror plasmas show that radial transport barriers can be produced by the use of off–axis ECH electron heating. This off–axis application of the ECH produces a radial electric field profile that controls the electron end losses. A cylindrical shell of high–energy electron is a layer at $r =$ 4-7 cm are formed from the barrier through the central cell and into the end region. 2 KeV but with low density relative to the bulk electrons. The electron end losses from the layer result in the formation of a positive ambipolar potential and disrupts confining ions locally near $r =$ 4-7 cm because of loss of negatively–charged electrons.

The potential hills in turn make the change in the sign of $E_r(r)$ at the local peak position of the potential hill near $r =$ 4-7 cm. The E_r reversal leads to the direction reversal of the sheared $E_r(r) \times B(z)$ drift flow in the azimuthal (theta) direction at the potential peak radius similar to the Internal Transport Barrier (ITB) in toroidal devices. As a result, turbulence and intermittent vortex–like structures in hot–ion plasmas are suppressed near the reversal layer. Such a sheared $E_r(r)$ formation and a separation between the internal and outward plasmas due to the layer at $r =$ 4-7 cm [*Cho, et al.* (2008)] results in the enhancement of temperature gradients in the layer. The thermal isolation effects make T_e and T_i increase in the internal region in the low–density plasma layer formed by the ECH barrier.

4.5.1 Shearless local ITB transport barriers in tokamaks produced by control of the radial electric field

In tokamaks, internal transport barriers are observed and measured when $q(r)$ has a minimum $q_{\rm min}$. They are produced by modifications of the toroidal plasma current profile. The internal

$q_{\min}$ surface separates the rational surfaces which reduces particle transport and improves plasma confinement [*Marcus, et al.* (2019)]. The triggering of the internal transport barriers and their dependence on the plasma profiles is a key nonlinear dynamics problem under current investigation. In tokamaks, internal transport barriers are produced by $q_{\min}$ from the plasma current profile by modifications of the plasma current profile, which reduces particle transport and improves plasma confinement. Progress to understand this reduction, the triggering of internal transport barriers and its dependence with the plasma profiles is an active research area [*Rowan, et al.* (2008)]. The onset of shearless invariant curves inside the plasma creates $q_{\min}$ internal transport barriers. A nonintegrable drift–kinetic model is used to describe particle transport driven by drift waves for large aspect ratio tokamaks to investigate the onset and growth of these internal transport barriers. Currently observed plasma profiles, shearless particle transport barriers can be triggered by properly modifying the ΔE_r electric field profile and the influence of nonresonant modes in the barriers onset [*Miura, et al.* (2017)]. In particular, a broken barrier can be restored by enhancing nonresonant modes $\Delta\phi_{m,n}(r)$ for $q(r_0) \neq m/n$ or eliminating $q = m/n$ surface.

Marcus, et al. (2019) develop the internal $q_{\min}$ creates the onset of shearless invariant curves inside the plasma which produces an internal transport barrier. A nonintegrable drift–kinetic model is used to describe particle transport driven by drift waves and to investigate the onset of these shearless barriers in tokamaks. Shearless particle transport barriers can be triggered by properly modifying the electric field profiles and the influence of nonresonant modes in the barriers onset [*Miura, et al.* (2017)]. In particular, the broken barrier can be restored by enhancing the neighboring nonresonant modes, as shown in theory and simulations by *Marcus, et al.* (2019).

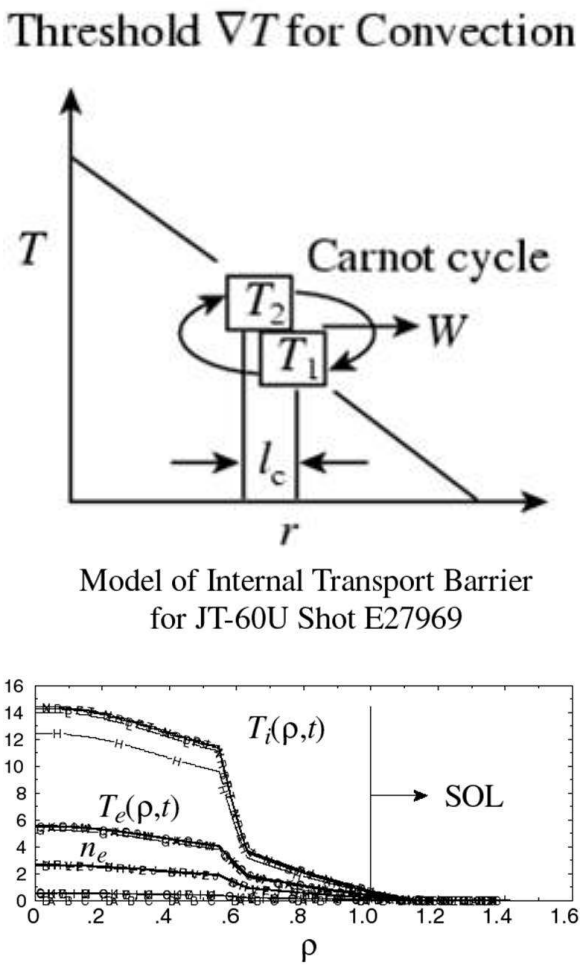

Figure 4.2: Boundaries of collisional and turbulent diffusivities.

4.6 The Planetary Magnetospheres of Earth, Jupiter and Saturn

4.6.1 Exploring the Solar System over 45 years from 1975 to 2020

The solar wind plasma expands from the Sun into the heliosphere plasma is approximately an isothermal expansion due to the rapid electron thermal transport. The speed and Mach numbers are roughly (i) at the Earth 400 km/s with $M_s = 4$, and (ii) at Jupiter 800 km/s with $M_s = 8$. Jupiter's magnetic moment $M_J = 2 \times 10^4\, M_E$ and radius where $R_J = 7.1 \times 10^4$ km. Jupiter's magnetopause radius is $R_{\rm mp} \simeq 45\, R_J = 3 \times 10^6$ km where $R_J = 7.1 \times 10^4$ km. The Earth's

magnetic moment is $M_E = 8 \times 10^{15}\,\mathrm{T.m^3}$. Jupiter has a high level of relativistic electrons (flux $> 10^6\,\mathrm{cm^{-2}s^{-1}}$) up to 20 MeV in energy. There is strong decimeter wavelength synchrotron radiation from the relativistic electrons in the magnetosphere of Jupiter [*Dessler* (1983)].

Voyager 2 launched in 1977, 16 days before Voyager 1. and Both V1 and V2 have traveled well beyond their original destinations. The spacecraft were built to last five years and conduct close–up studies of Jupiter and Saturn. However, as the mission continued, additional flybys of the two outermost giant planets, Uranus and Neptune, proved possible. As the spacecraft flew across the solar system, remote–controlled reprogramming was used to give the Voyagers with greater capabilities than they possessed when they left Earth. Their lifespans have stretched to 41 years, making Voyager 2 NASA's longest running mission.

4.7 Jupiter and Saturn

Jupiter is the largest planet with four large moons first discovered by Galileo [*Lawson* (2002)]. Saturn is the second largest planet with a complex set of plasma rings orbiting the fast–spinning planet.

Bibliography

[1] Nakmura, Y., Kobayashi, M., Yoshimura, S., Tamura, N., Yoshinuma, M.,Tanaka, K., Suzuki, C., Peterson, B. J., Sakamoto, R., Morisake, T. and the LHD Experiment Group (2014). Impurity shielding criteria for steady–state hydrogen plasmas in the LHD, a heliotron–type device, *Plasma Phys. Control. Fusion* **56**, p. 075014, https://doi.org/10.1088/0741-3335/56/7/075014.

[2] Nakmura, Y., Tamura, N., Kobayashi, M., Yoshimura, S., Suzuki, C., Yoshinuma, M., Goto, M., Motojima, G., Nagaoka, K., Tanaka, K., Sakamoto, R., Peterson, B. J., Ida, K., Osakabe, M., Morisake, T. and the LHD Experiment Group (2017). A comprehensive study on impurity behavior in LHD long pulse discharges, *Nucl. Mat. Energy* **12**, pp. 124–132, https://doi.org/10.1016/j.nme.2016.11.005.

[3] Yoshinuma, M., Ida, K., Yokoyama, M., Osakabe, M. and Nagaoka, K. (2010). Charge–exchange spectroscopy with pitch–controlled double–slit fiber bundle on LHD, *Fusion Sci. Tech.* **58**, pp. 375–382, https://doi.org/10.13182/FST10-A10823.